ARTICLE

Measuring Interactions of DNA with Nanoporous Protein Crystals by Atomic Force Microscopy

Dafu Wang, a,b Julius D. Stuart, a Alec A. Jones, d Christopher D. Snow, a,b,c,d and Matt J. Kipper a,b,d*

Received 00th January 20xx, Accepted 00th January 20xx

DOI: 10.1039/x0xx00000x

Crosslinked porous protein crystals are a new biomaterial that can be engineered to encapsulate, stabilize, and organize guest molecules, nanoparticles, and biological moieties. In this study, for the first time, the combined interactions of DNA strands with porous protein crystals are quantitatively measured by high-resolution atomic force microscopy (AFM) and chemical force microscopy. The surface structure of protein crystals with unusually large pores was observed in liquid via high-resolution AFM. Force-distance (F-D) curves were also obtained using AFM tips modified to present or capture DNA. The modification of AFM tips allowed the tips to covalently bind DNA that was pre-loaded in the protein crystal nanopores. The modified tips enabled the interactions of DNA molecules with protein crystals to be quantitatively studied while revealing the morphology of the buffer-immersed protein crystal surface in detail, thereby preserving the structure and properties of protein crystals that could be disrupted or destroyed by drying. The hexagonal space group was manifest at the crystal surface, as were the strong interactions between DNA and the porous protein crystals in question. In sum, this study furthered our understanding of how a new protein-based biomaterial can be used to bind guest DNA assemblies.

1. Introduction

Protein crystals are a unique nanomaterial with highly ordered and well-defined three-dimensional structures. The enormous variety of crystal structures provides access to uniquely tunable and evolvable nanomaterials. We are interested in the unusual crystals of a putative isoprenoid binding protein from Campylobacter jejuni (Genebank ID: CJ0420, Protein Data Bank (PDB) code: 5w17), which we refer to as CJ. This protein readily and rapidly assembles into highly porous protein crystals (Fig. 1).1-4 Each unit cell within these crystals contains 12 protein monomers arranged according to the P622 space group. CJ crystals are hexagonal three-dimensional arrays with 13 nm-diameter nanopores (18 nm pore-center-tocenter) that are aligned along the z-axis. The major nanopores extend from the top of the crystals to the bottom, reminiscent of a honeycomb. Once crosslinked, these materials offer an unusual combination of macroscopic stability, nanoscale precision, and a high capacity to uptake macromolecular guests. Previous studies have shown the capability of large-pore protein crystals for the capture of guest nanoparticles and proteins. 1, 4

The uncommonly large pores of CJ crystals also provide ample space for double-stranded DNA (dsDNA, hereinafter as DNA), with a diameter of 2 nm, to be loaded and stored within each 13 nm-diameter nanopore (Fig. 1). We have observed strong affinity for nucleic acids to adsorb to the crystal interior. In this regard, the porous crystal shares a key attribute of viral capsids and spores. Efforts are underway to exploit this effect for applications including information storage and DNA delivery. We are also interested in determining if it is possible to use the extraction of polymers from the crystal nanopores by mechanical force as the basis for a force-sensitive signal transduction scheme.¹

To date, the basis of the observed, favourable nucleic acid/protein interaction has not been clear. Here, to investigate, we seek to directly quantify the attraction between DNA and the crystal nanopores. In this study, the characterization of crystals' surface morphology is also critical because the surface is where the crystal interacts with its environment. Guest molecules that are transported into or out of the crystal nanopores must traverse the interface represented by the crystal surface. Atomic force microscopy (AFM) is a powerful tool for the study of materials' surfaces, providing molecular-scale resolution of surface features.5-13 Unlike electron microscopy, AFM in buffered solutions affords opportunities for in situ imaging and molecular force measurements of fragile biomolecules in native conformations. 12-17 In addition to revealing the surface structure, AFM can also apply small controlled forces (pN level) to determine mechanical properties of materials and can characterize molecule-level adhesion events using force-distance (F–D) curves.^{12, 17-22}. Accordingly, AFM studies of protein crystals have included the visualization of mechanical behaviors, 23 mapping the surface morphology on 2-D crystal substrates,8 imaging protein crystals in liquid phase,14 and high-speed high-resolution imaging of crystallization dynamics.²⁴ Using solution AFM to characterize the

^{a.} School of Advanced Materials Discovery, Colorado State University, 1617 Campus Delivery, Fort Collins, CO 80523, U.S.A.

b. Department of Chemical and Biological Engineering, Colorado State University, 1370 Campus Delivery, Fort Collins, CO 80523, U.S.A., E-mail:

c. Department of Chemistry, Colorado State University, 1872 Campus Delivery, Fort Collins, CO 80523, U.S.A.

d. School of Biomedical Engineering, Colorado State University, 1301 Campus Delivery, Fort Collins, CO 80523, U.S.A.

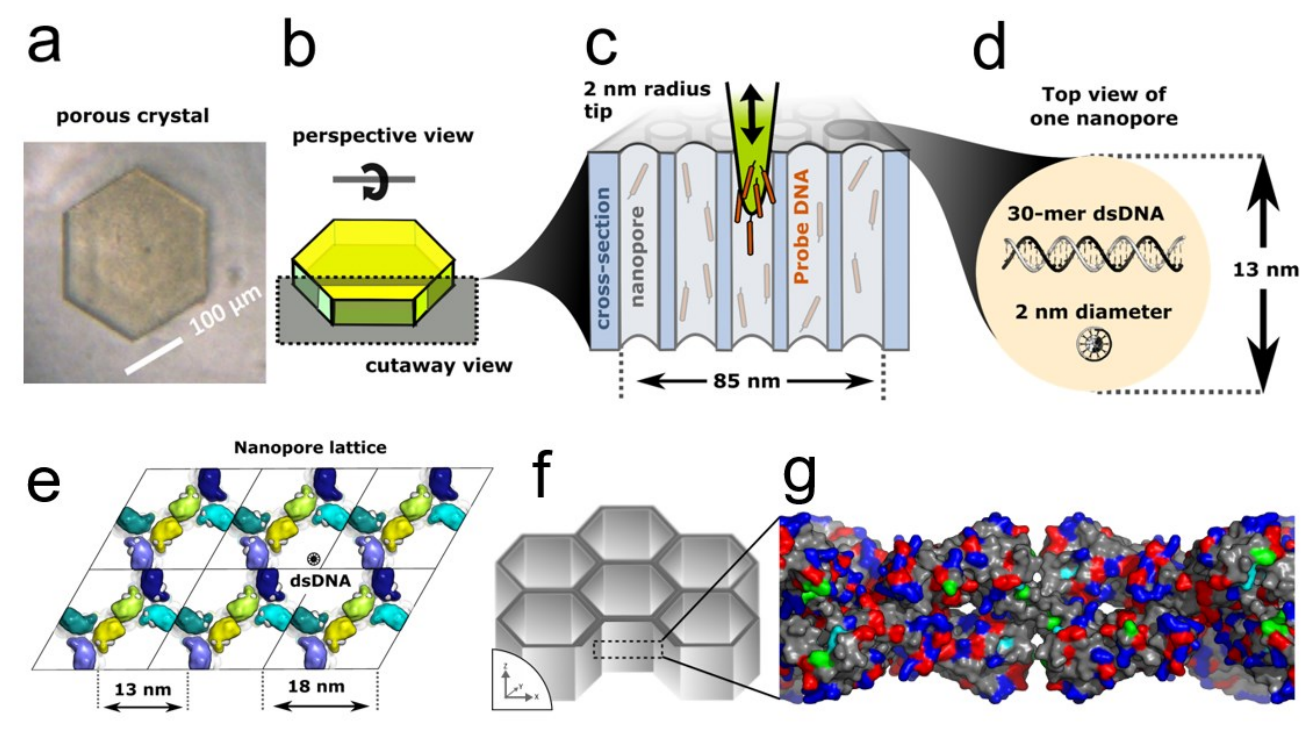


Fig. 1. A periplasmic protein, "CJ", from *Camphylobacter jejuni* forms (a) porous protein crystals that we stabilize via crosslinking. (b) Typical crystals are hexagonal prisms. (c) A hexagonal array of 13 nm-diameter nanopores runs from the top to the bottom of each crystal. Modified DNA molecules can be loaded into these nanopores and then pulled out using activated AFM probes capable of covalently bonding to the DNA. The top face of the crystal may then be probed using chemical force microscopy with DNA-modified AFM tips. 1-4 (d) Within each 13 nm-diameter nanopore, it is possible to fit numerous DNA double helices parallel to the host nanopore axis since DNA has a 2-nm diameter. A 30-mer DNA almost spans the nanopore diameter. (e) A top view of two adjacent nanopores (PDB code 5w17), with guest DNA to scale. (f) crystal schematic with nanopores cut away, and (g) zoomed in slice of nanopore side wall illustrating presence of ionizable amino acid. Carboxylic acids (Asp, Glu) are shown in red. Arginines are shown in cyan. Lysines are shown in dark blue. Notably, some of the Lysine sidechains have likely lost their positive charge by participating in glyoxal crosslinks. Glyoxal crosslinked crystals tend to diffract to modest resolution ~3.5Å and surface lysine sidechains tend to be highly mobile. These two factors, as well as heterogeneity within the crystal, prevent us from assessing which lysines are likely to retain their positive charge. Finally, the figure shows histidine sidechains in green. Both the N-and C-terminus contain flexible regions that are not pictured in this crystal structure. The flexible C-terminal histag (not pictured) is of particular interest as a possible participant in DNA binding. Image was created by PyMOL.

protein crystals enables the periodicity and morphology of crystals to be studied in their mother liquid, thereby preserving the as-grown periodic protein crystal structure, which can be disrupted or destroyed by drying.¹⁴

While the bulk structure of CJ protein crystals has been elucidated by X-ray crystallography, the surface morphology of CJ protein crystals with unusually large pores has not yet been characterized at the resolution of the pore-containing unit cell. Therefore, prior to this study, the degree of nanopore uniformity on the surface was unknown. Surface roughness and nanopore obstructions are features that could impact the future engineering of protein crystals as hosts for guest molecules such as DNA. The present work was therefore undertaken to characterize the CJ protein crystal surface by AFM, and to determine the interactions of guest DNA with the protein crystal. To be clear, the current study is not designed to isolate the interaction of a single DNA molecule with the host crystal. Instead, multiple DNA strands are captured by the AFM tip allowing the study of multivalent DNA interactions with the host crystal. Many future guests of interest such as DNA-coated particles, assembled DNA tiles, DNA origami, plasmids, or even long dsDNA oligos are expected to interact with the crystal via multiple DNA segments. We are particularly interested in the scenario where appropriately sized

nanoparticles with surface conjugated DNA may be used to reversibly block the nanopores.

In our study, among other experiments, we preloaded DNA into the nanopores of CJ crystals. Modifying the AFM tip with dithionitrobenzoic acid provides a covalent attachment site for thiolterminated DNA to be strongly connected by disulfide bonds to the AFM tip. Ideally, multiple dsDNA blocks present within the crystal can be captured by the AFM tip and pulled out of the protein crystal pores, or pulled off of the protein crystal surface. As illustrated in Fig. 1C, a sharp activated AFM tip is capable of penetrating deeply into the nanopores and thus capturing multiple DNA molecules. The captured DNA then persists on the AFM tip throughout subsequent imaging, enabling measurements of the molecular forces between DNA and protein crystals. During the imaging process, the Bruker Bioscope Resolve AFM operated in PeakForce QNM mode, records a force-distance (F-D) curve at each pixel in the scanned area of the sample surface. Thus, every pixel in the AFM image contains an F-D curve. We were able to gather hundreds of thousands of (F-D) curves in a single imaging experiment without interrupting the imaging process. We were also able to exactly locate the force curves on the images, to gain a better understanding of the connection between the mechanical behaviors and the morphology of the surface.

For comparison, we also imaged the crystals with tips that were covalently modified with DNA prior to imaging. For the first time, we showed that the interactions of AFM-tip-conjugated DNA with a porous protein crystal can be directly and quantitively measured. This study will enable us to tune protein crystals and solution conditions for DNA storage and release. The current multivalent DNA interaction data and analysis will also guide the design and interpretation of future single-molecule studies of this system.

2. Experimental

2.1 Materials

A Millipore Synthesis water purification unit was used to obtain 18.2 $\,$ M Ω cm water, used for making all aqueous solutions. 3-(TrimethoxysilyI)propylamine (APTMS) for molecular vapor deposition (MVD) was purchased from EMD Millipore Corp. Traut's reagent (2-iminothiolane) used for tip modification was purchased from Chem-Impex International, Inc. 5,5'-Dithiobis-(2-nitrobenzoic acid), (DTNB, Ellman's reagent) were purchased from Thermo Fisher Scientific, Inc.

2.1.1 CJ Crystal Growth Details of the protein crystal growth are provided in the Supporting Information, section S2.1.1.

2.1.2 CJ Crystal Crosslinking and Immobilization In this study, medium-large CJ protein crystals were used, with a typical diameter of 400 μm to 700 μm , and typical height of 50 μm . The crystals must be crosslinked to facilitate later solvent exchange. Crystals were transferred (using a nylon crystallography loop, Hampton Research) from their growth well into a drop of 4.2 M trimethylamine N-oxide (TMAO), 0.175 M H_2SO_4 at pH = 7.5, to wash for a minimum of 20 min. A drop of 390 μ L of 4.2 M TMAO, 0.175 M H_2SO_4 at pH 7.5 plus 10 μL of 40% glyoxal crosslinker was then prepared. Crystals were manually transferred into crosslinking solution and covered for 2 h. Meanwhile, a drop of 380 μL 0.1 M sodium citrate, 0.15 M NaCl at pH 5.0, 10 μL of 50% hydroxylamine, and 10 μL of 40 mg/mL dimethylamine borane complex was prepared. The crosslinked crystals were transferred to this "quenching" solution to eliminate reactive groups. After 8 hours in the quenching solution, crystals were ready to be used or stored. Crystals were stored in 4.0 M TMAO and washed briefly in water or adsorption buffer (30 mM KCL, 10 mM MES, pH = 6.0) prior to use. The surfaces of crystals were weakly negative charged after crosslinking, with a negative zeta potential. (Supporting Information Fig. S10). The interior of the protein crystal pores contains both positive and negative ionizable groups. The modest negative surface potential and mixed charges of the pores suggests that simple electrostatic attraction is not the primary driving force for DNA adsorption. Empirically, the lack of DNA desorption in high salt washes (data not shown) further supports the idea that DNA binding is not dominated by electrostatic interactions that can be screened at high salt.

For AFM experiments (described below), CJ crystals were immobilized on glass-bottom petri dishes (Willco Wells) employing a UV-curable glue (Bondic Inc.). The top of a crystal probe (Minitool HR4-217) was used to transfer a drop of UV-curable glue onto the surface of a petri dish (Ted Pella, Inc. 14025-20). The glue was gently and evenly spread on the dish surface to make the layer of glue as thin as possible. CJ crystals were transferred to the glue with a loop. Critically, the crystal was transported inside a tiny drop of buffer, such that the crystal was not desiccated. The UV-glue was viscous and did not noticeably mix with the buffer. The glue was then cured by exposing to UV-light LED (Bondic SK001) from above for 10 s. The glue cured after about 2 min, after which additional drops of buffer (typically ~5 mL) were added to the dish to prevent the crystal from drying.

2.2 AFM Tip Modification

Bruker's ScanAsyst Fluid+ tips were modified to covalently attach DNA (Fig. S1). These tips have a slim shape with estimated tip radius as small as 2 nm, and a silica surface layer. To clean the tip surface and to activate the hydroxyl groups on the silica surface of the tip, AFM tips were placed in O_2 plasma chamber (Plasma Etch. Inc) with a 200–300 mTorr total pressure inside the chamber, and the power setting was adjusted to 38 W for 5 min.²⁵ Then, molecular vapor deposition (MVD) was used for amino-silane treatment of the surface of AFM tips. AFM tips were placed into a 1-L polypropylene jar. Two mL of APTMS aminosilane was added to a 10-mL scintillation vial, also placed in the polypropylene jar. The polypropylene jar was sealed using a screw cap lid, and placed in a 60 °C oven for 60 min. This allows the surface of the AFM cantilever tip to be modified with the APTMS by MVD forming an aminosilane layer anchored to the surface.²⁵

Traut's reagent (2-iminothiolane) reacts spontaneously with primary amines (-NH₂) at pH = 7.0 to introduce sulfhydryl (-SH) groups. We used this reaction with 1 mM Traut's reagent at room temperature in 50 mM KCl solution. ²⁵ To activate the AFM tips for binding thiol-terminated DNA, AFM tips were modified using dithionitrobenzoic acid. Specifically, the remaining 2-iminothiolane solution was replaced with excess 5,5'-dithiobis-(2-nitrobenzoic acid), (DTNB, Ellman's reagent, 500 μ M) in a 0.1 M dipotassium phosphate and sodium bicarbonate buffer (pH = 8). Activating the AFM tip with DTNB enables thiol-terminated DNA to be reversibly and covalently bound to the AFM tip via a thermodynamically favored disulfide exchange reaction.

Each step in the surface modification of the AFM tips was evaluated by X-ray photoelectron spectroscopy, using a Physical Electronics 5800 spectrometer (Chanhassen, MN). This XPS uses a monochromatic Al K α X-ray beam source (hv = 1486.6 eV), hemispherical analyzer, and multichannel detector. The binding energy scales for the samples were referenced to the aliphatic

contribution of the C1s peak at 284.8 eV. High-resolution spectra of the N1s, S2p and P2p envelopes were acquired with 0.1 eV steps, and an X-ray spot size of 800 μm . Given this size, the XPS spectra report surface chemistry of the tip, cantilever, and probe, but the tip is composed of the same material as the probe. Analyses were performed at a photoelectron take-off angle of 45°. Peak fitting of the N1s and S2p envelopes was performed in MultiPak (Ulvac-Phi, Inc.) using Gaussian/Lorentzian peaks and a Shirley background correction. The morphology of both unmodified and modified AFM tips was also imaged by field emission scanning electron microscopy (FESEM, JEOL JSM-6500F).

2.3 DNA Loading and AFM Probing

We operated the AFM (Bruker Bioscope Resolve, mounted on a spinning-disc confocal microscope built around a Nikon Eclipse TiE) in quantitative nano-mechanics (QNM) PeakForce Capture mode. All images and force curves were collected using ScanAsyst Fluid+ tips (Bruker). Crystal imaging was performed in TE (Tris-EDTA) / DI H_2O buffer (5 mM Tris-HCl, 1 mM EDTA, pH = 7.5) with crystals affixed to the bottom of a glass petri dish. The AFM line scan rate was set to 1.0 Hz and the peak force tapping frequency was set to 1.0 kHz. The peak force set point was set to 2 nN. Notably, the force used here is large with respect to the forces used by investigators who use optical trap experiments to study the interactions of DNA molecules with other partners. Specifically, Dario Anselmetti et al. used peak force of

800 pN, while Stuart Lindsay and coworkers used a peak force of 160 pN. 26,27 The QNM PeakForce Capture mode is based on force-versus-distance measurements in which the tip oscillates sinusoidally, at a frequency far below the resonance frequency of cantilever, f_0 . This mode provides a high-resolution peak-force mapping as well as sensitivity to record nano-mechanical behaviors at high spatial resolution. 28 Tip-sample interactions are measured with pN-resolution by the deflection of the cantilever. Analysis of the AFM data was performed in NanoScope (Bruker, Inc.), Origin (OriginLab, Inc.), Python (Version 2.7), and Matlab (Version 2019).

The protein crystal sample was imaged by both AFM (unmodified tip), and confocal microscopy to confirm immobilization and to verify that the crystal surface was clean. When crystals were incorrectly prepared, their surfaces could be obscured by aggregated protein. To ensure that the crystals were competent to uptake DNA, we used time-lapse confocal microscopy (z-stack imaging) to monitor and confirm the loading of fluorescently labeled DNA. First, the CJ crystals were photobleached to prevent interference from background fluorescence. Prior to DNA loading, as a control experiment, the protein crystal was imaged using an activated AFM tip (terminated with the dithionitrobenzoic acid, but without DNA) in TE buffer (Condition D in Fig. 2). Then, the TE buffer solution was replaced by 100 μL 50 μM 30mer-DNA with two terminal thiol groups (sense strand, 5'-3': /5ThioMC6-D/TAG GCG ACT CGA CGG TCT TAC GCG TTA CGT, anti-sense strand, 5'-3': ACG TAA CGC GTA AGA CCG TCG AGT CGC CTA) in TE buffer. Prior to loading, a stock of the same 30-mer

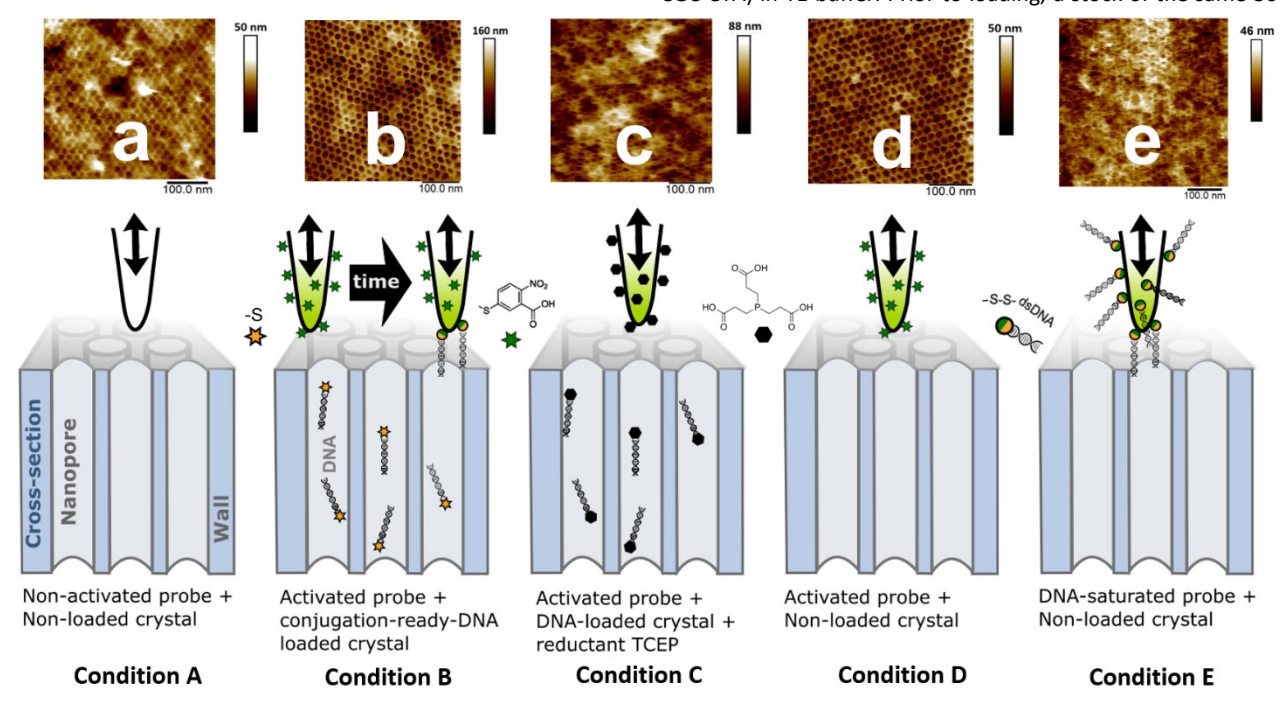


Fig. 2 Force microscopy schematic illustration of AFM tips with protein crystals. The condition indices A-E in this figure correspond to the indices in Figure 9. All conditions are shown accompanied by the corresponding surface morphology AFM image. (a, condition A) The non-activated AFM tip is white. (b, condition B) The activated AFM tip is green and covered with green stars to represent the thiol-reactive Ellman's reagent leaving group. DNA oligos preloaded into the crystal have a terminal thiol group (orange stars). We expect the tip to conjugate and "fish" out multiple oligos at the outset of the experiment. (c, condition C) The reducing agent TCEP (black hexagons) should reverse any disulfide bond formation between the DNA and the activated AFM-tip, yielding detached oligos. (d, condition D) A no-DNA control. (e, condition E) In contrast, an activated AFM tip can be saturated with DNA molecules in solution prior to encountering the crystal.

DNA was fluorescently labeled with **TAMRA** (carboxytetramethylrhodamine) (Integrated DNA Tech.) for 30 minutes. During loading, 10% (90%) of the DNA was TAMRA-labeled (unlabeled). Next, after washing three times with TE buffer (30 min per wash), the samples were incubated with 100 µL of 50 µM tris(2carboxyethyl)phosphine (TCEP) in TE buffer for 30 minutes to reduce disulfide bonds. After reduction of disulfide bonds with TCEP, the DNA-loaded crystal was again washed with 1 mL TE buffer for 30 min, three times, to remove the TCEP. Retention of the DNA was confirmed by confocal microscope imaging after each wash step. The DNA-loaded crystal was then imaged with an activated AFM tip (Condition B in Fig. 2), and F-D curves were collected at each pixel in the AFM image.

As a control experiment, the procedure for loading the protein crystal described above was repeated using DNA previously reacted with 100 μL of 14 mM iodoacetamide (in 100 mM Tris-HCL buffer, pH = 8.3). Ideally, iodoacetamide will permanently "cap" the DNA to ensure that it cannot covalently bind to the activated AFM tip. The crystal loaded with deactivated, "capped" DNA was imaged with an activated AFM tip (Condition C in Fig. 2).

AFM imaging and F-D curve collection was conducted for five different experimental conditions as described above, using combinations of un-modified, activated, and DNA-modified tips and either loaded or unloaded protein crystals. The five experimental

conditions are: (condition A) un-modified AFM tip on an unloaded crystal, (condition B) activated AFM tip on a crystal loaded with thiol-bearing DNA, (condition C) activated AFM tip on a DNA-loaded crystal in the presence of TCEP and iodoacetamide, (condition D) activated AFM tip on an unloaded crystal, and (condition E) 30-mer DNA-modified AFM tip on an unloaded crystal. From each AFM image, F-D curves were manually assigned to one of two classes, corresponding to protein crystal surface features: pores and walls.

3. Results and Discussion

3.1 AFM Imaging on Surface Morphology

AFM imaging resolves details of the porous CJ crystal surfaces (Fig. 3). The CJ crystal surface presents a regular honeycomb pore/hole structure consistent with single-crystal X-ray diffraction data (PDB entry: 5w17).¹⁻⁴ The observed surface structure of CJ protein crystals did not change significantly when imaged with different tip modifications. The CJ crystal surface structure was regular and uniform, with features that are consistent among different protein crystal samples. Notably, the previously reported structure obtained from X-ray diffraction (13 nm-diameter pores in a hexagonal array) is confirmed by AFM to be manifested at the crystal surface.^{1, 2, 4} The AFM z-height image is a convolution of the surface height and the geometry of the AFM tip. A one-dimensional z-height trace across the centers of multiple pores is shown in Fig. 3(c).

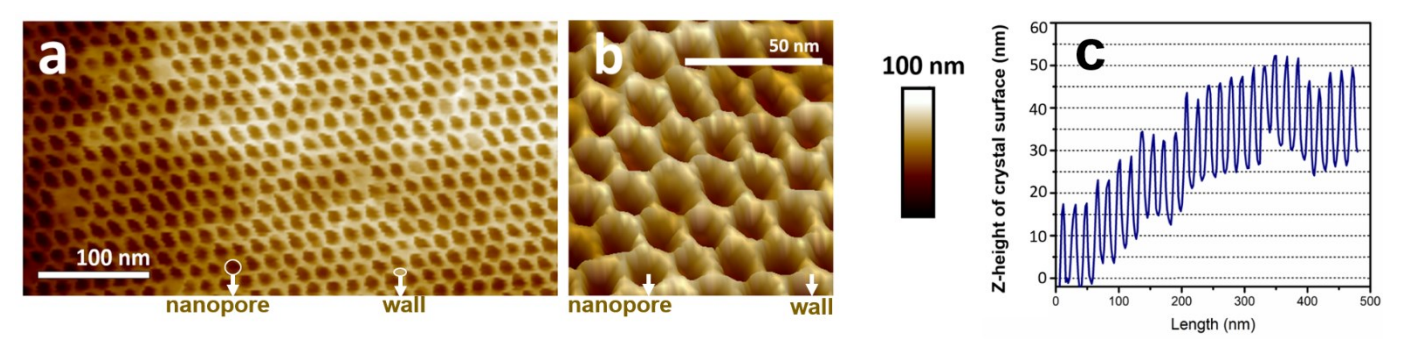


Fig. 3 (a) AFM image of CJ crystal surface (b) 3D rendering of a portion of the height data from Fig. 3 (a) (c) a side height section of crystal surface from Fig. 3 (a), across the center of multiple pores.

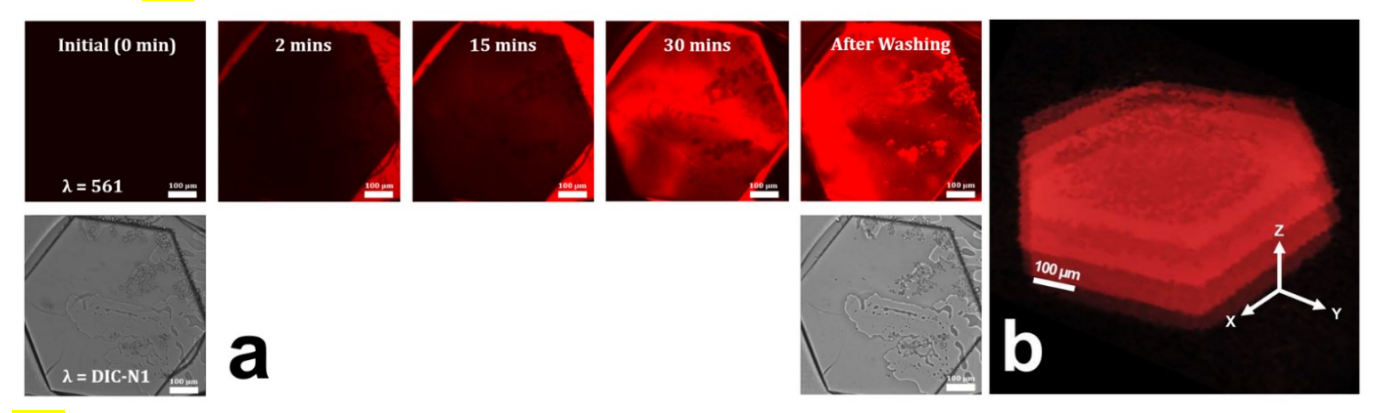


Fig. 4 (a) Confocal microscope images of fluorescent DNA loading into a CJ protein crystal (0-30 minutes time-lapse), and after washing with TE to reduce DNA outside the nanopores. (b) The 3-D distribution (z-stack) of 5 confocal microscopy images of labeled DNA after TCEP washing. The z-stack planes are separated by 10 μm in the z direction.

When the tip is located over the center of a pore, a minimum in the z-height is recorded, and when the AFM tip is located over the center of the wall separating two pores, a maximum in the z-height is recorded.

3.2 Modification of AFM Tips

The spring constant and tip diameter of each tip used for imaging and quantitative measurements were quantified using hardness and surface roughness standards. The spring constant of a fully modified AFM tip used to collect data for this paper was 0.94 N/m, with an estimated tip diameter of 5.09 nm (ETD, data from NanoScope). Modified and unmodified tips were also imaged by field emission scanning electron microscopy (FESEM, Supporting Information Fig. S3), confirming that the silanization and subsequent chemical modifications do not alter the tip geometry on a macroscopic scale that might be observed via SFM.²⁹

X-ray photoelectron spectroscopy (XPS) was used to characterize the modification of AFM tips. In this study, the high-resolution XPS spectra, as well as the changes of N1s, S2p, and P2p peaks confirm each step of modification chemistry of Section 2.2. Activation of the tip with excess 5,5'-dithiobis-(2-nitrobenzoic acid) (DTNB) enables

the 30-mer DNA to be covalently bound to the AFM tip via disulfide bonds with the thiol-terminated DNA. This enables DNA to be bound and extracted from nanopores of CJ crystals by the AFM tip. The existence of disulfide, thiols, and O-P-O₃ phosphate envelopes confirm that DNA is successfully modified to the surface AFM tip. ³⁰, ³¹ Complete and detailed XPS results are provided in the Supporting Information as Fig. S2.

3.3 DNA Loading

Absorption of the DNA into the crystal following immersion in guest DNA solution containing 10% 30-mer DNA fluorescently labeled with TAMRA is confirmed by confocal microscopy. Throughout loading, fluorescence intensity increased in the CJ protein crystal interior. After washing with TE buffer and 25 mM TCEP in TE buffer, confocal microscope imaging shows the retention of guest DNA (Fig. 4). From XRD data, each unit cell has a free volume of 1413 nm³ (1.413×10 $^{-15}$ μL). $^{1.4}$ Therefore, a medium-large crystal (400 μm diameter, 50 μm height) would contain about 3.7 trillion unit cells. According to the confocal microscopy imaging, the estimated height of this particular protein crystal was 50 μm , with a diameter of 745 μm , and the crystal's side length was 363 μm .

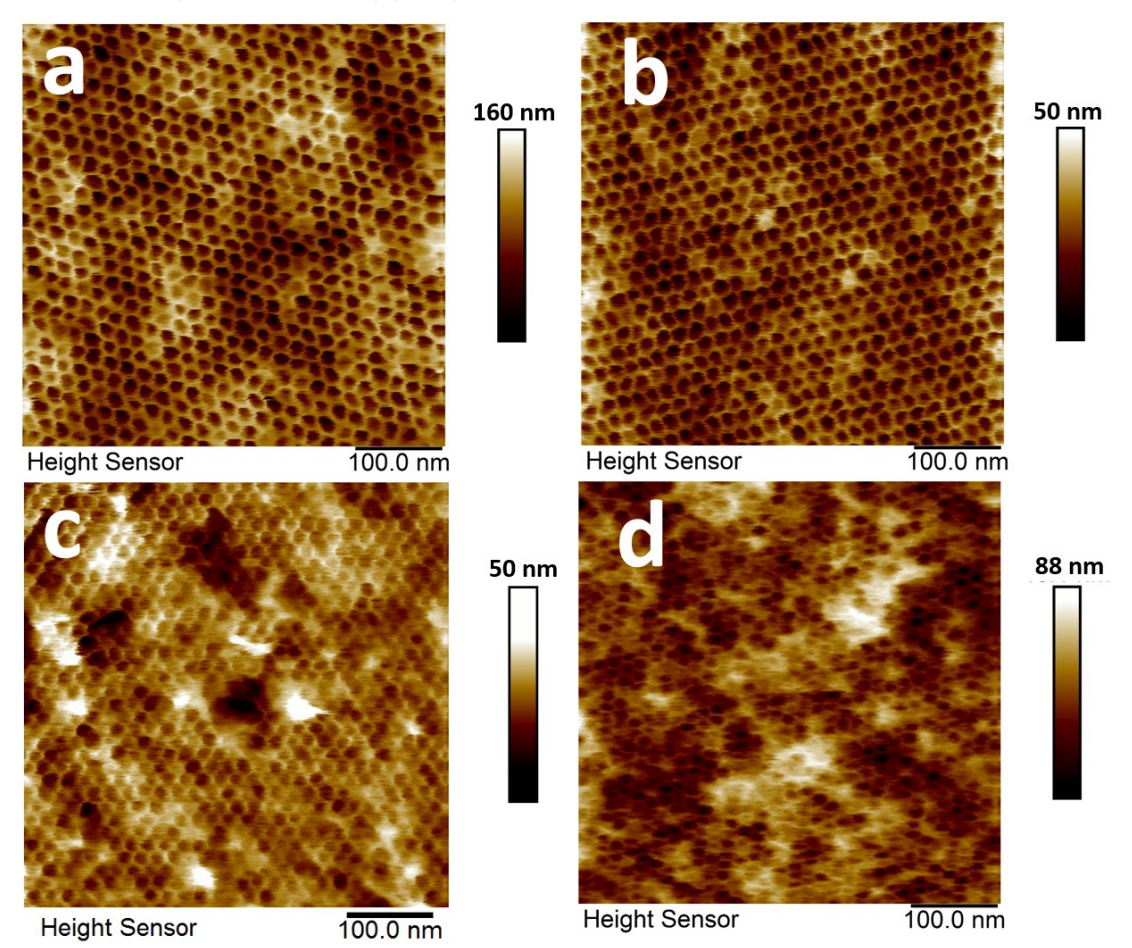


Fig. 5 AFM images of (a) a crystal loaded with DNA imaged using an activated AFM tip, (b) an unloaded crystal imaged with an activated AFM tip, (c) an unloaded crystal imaged with a non-modified AFM tip, and (d) a crystal loaded with DNA imaged with an activated tip after deactivating thiols with iodoacetamide.

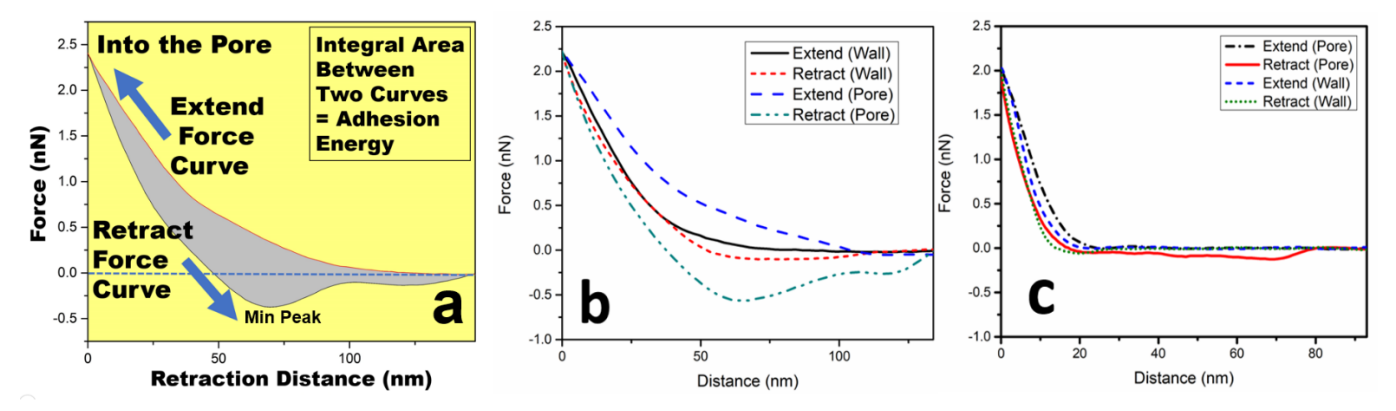


Fig. 6 (a-b) Representative examples of force-distance (F-D) curve obtained using a modified AFM tip on crystal loaded with DNA, (a) F-D curve of a nanopore center, (b) comparison of F-D curves of representative pore and wall pixels. (c) F-D curves obtained using a DNA-modified AFM tip on an unloaded crystal obtained from both pore and wall pixels.

We can obtain an estimate for the 30-bp DNA concentration inside the crystal by comparing the relative volume of the crystals and the supernatant as well as the relative fluorescence intensity. Specifically, when we quantify the volume of the solution outside the crystal, the volume and concentration of DNA outside the crystal at the experiment outset (100 μ L, 50 μ M), the estimated volume of the crystal (0.0237 µL), and the relative fluorescence intensity of the DNA inside and outside the crystal, we can use a material balance to estimate a final average intra-crystal concentration of 138.86 µM (with a maximum of 205.77 μ M) (Supporting Information Table S3). At this DNA loading density, with the known unit cell volume (1413 nm³), we can estimate that the average concentration is approximately 0.117 DNA molecules per unit cell within the crystal (maximum 0.174 DNA molecules per unit cell), if guest DNA molecules are distributed randomly throughout the crystal. Since the CJ unit cell is ~5 nm tall, and a 30-bp DNA is ~10 nm tall, we envision that DNA would not be crowded within the crystal but would be commonly encountered by chance within the nanopores.

3.4 Interaction of DNA and CJ Protein Crystals

Upon interaction of the activated AFM tip with the DNA-loaded protein crystal, the AFM tip can be used to remove DNA from the protein crystal pore or surface, and to measure the force of the interaction. In PeakForce QNM mode, the AFM captures and records a force-distance (F-D) curve at each pixel of the scanned area of the image. During this study, we collected hundreds of thousands of F-D curves by AFM under different conditions. To measure the F-D curves and obtain the adhesion energy of DNA with the pores and walls of CJ protein crystals, five different combinations of tip modification (Fig. S1) and DNA loading were used as shown in Fig. 2. Respectively, each combination contains two types of areas: pores and walls. Fig. 5 shows that loading DNA in the nanopores of CJ protein crystals does not substantially change the surface morphology of crystals. Varying levels of surface aggregation apparent among the images in Fig. 5 are likely due to crystal-to-crystal variation in growth, washing, and crosslinking processes. The high-resolution images obtained for each condition provides confidence that our AFM parameters and sample immobilization method provide data of suitable quality to further investigate the interactions between DNA and the host CJ crystals.

The adhesion energy between the DNA and the CJ protein crystals at each tap can be calculated as the integral of the area between the extend force curve and retract force curve (corresponding to the grey area in Fig. 6 (a)). The measured interaction for this representative pore pixel has a larger force volume, a longer distance of force measurement, as well as a higher adhesion energy than the wall pixel. Remarkably, it can be seen in Fig. 6 (a) that the interaction of the AFM tip with the protein crystal in both the extend and retract portions of the curve occurs over more than 100 nm in the zdirection. We hypothesize that the crosslinked protein crystal surface deforms elastically under the approximately 2 nN peak force used here (Fig. 7 (c)). Axial and lateral deformation may contribute to the penetration distance, and induce energy changes by performing extra work. Notably, the length scale of interaction is significantly reduced for an AFM tip that was DNA- modified and used to probe a crystal that is not incubated with probe DNA (Fig. 6 (c)).

We randomly selected 20 sets of F-D curves on pores and walls for each of the five experiments described in Fig. 2 (200 sets of F-D curves total). To account for different distances of tip penetration into the pores, the average adhesion energy in the pores was normalized by an estimated average pore area of interaction, calculated by approximating the area of a 13-nm diameter cylindrical pore ($A_{pore\,surface} = 13nm \cdot h \cdot \pi$) at the local depth of penetration h of the tip (Fig. 7 (b)). When there was no DNA loaded in the protein crystals, there was no significant difference between the average adhesion energy of pore center pixels and wall pixels, when measuring with a modified AFM tip. When using non-activated AFM tips to measure the adhesion energy on unloaded protein crystals, both pore and wall pixels had their lowest mean adhesion energy among tested conditions (condition A in Figs. 2 and 7). The interaction measured by the modified AFM tip for pore center pixels for the CJ protein crystal loaded with DNA has the highest average adhesion energy (condition B in Figs. 2 and 7). Among the sample curves, the highest adhesion energy for this condition reaches 8.08 × 10^{-2} fJ, and the average adhesion energy is 5.12 × 10^{-2} fJ. This adhesion energy is much larger than the adhesion energy for the unloaded crystal and unmodified AFM probe, indicating that the adhesion of the DNA to the protein crystal is being measured. Furthermore, in many cases the total interaction persisted over a remarkably large total tip travel distance of about 150 nm. The tipto-pore center interaction was reduced when putative disulfides

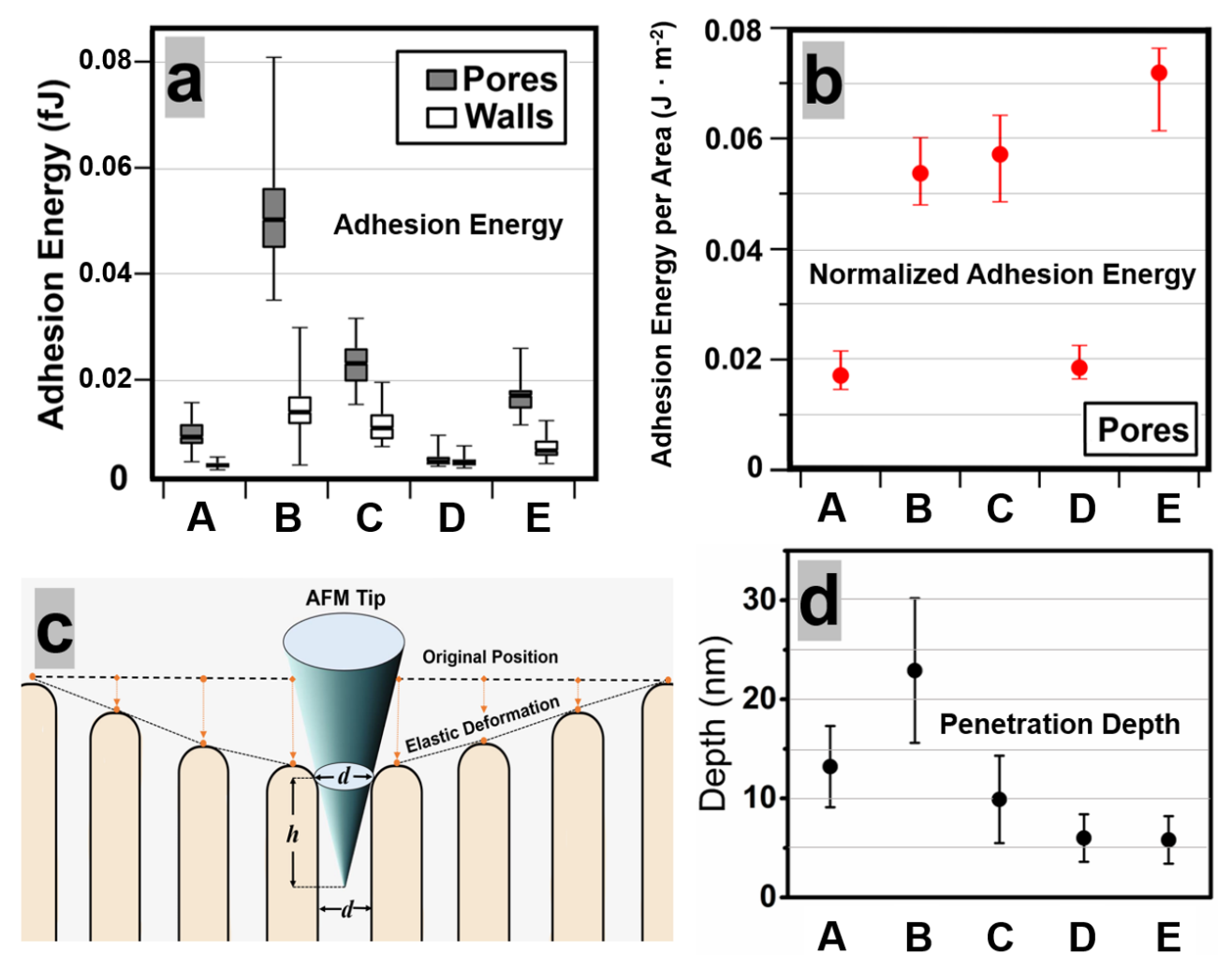


Fig. 7 Adhesion and penetration for the various AFM probe conditions (A,B,C,D,E) illustrated in Fig. 2. A: naked probe, B: activated DNA-capturing probe, C: after reductive DNA cleavage, D: activated probe lacking DNA, and E: probe saturated with DNA in solution. (a) Box plot (min, 25th, 50th, 75th percentiles, and max) of the adhesion energy for 20 pore center pixels and 20 wall pixels for each of the experiments depicted in Fig. 2. and (b) adhesion energy in the pores, normalized by the interacting pore area (adhesion energy divided by average area computed from the depth of penetration of the AFM tip into the pore) for 20 pore center pixels. The conditions labeled A-E here correspond to the conditions described in Fig. 2. (c) schematic showing axial elastic deformation of the protein crystal surface (lateral deformation is not illustrated), and the AFM probe penetration into the pores, "d" represents the effective diameter of a nanopore, "h" represents the penetration depth of the probe into the pore. (d) mean and standard deviation of probe penetration depth into the nanopores for experiments at conditions A to E. Conditions and detailed data are listed in the Supporting Information Table S2 (a-c)

were reduced to thiols with TCEP and capped with iodoacetamide (case C in Figs. 2 and 7), while the average adhesion energy at the wall areas did not change much upon reduction. In addition, we also measured the interaction between an inactivated AFM tip with a DNA-loaded crystal (Supporting Information Fig. S4). The experiment showed similar results of force and adhesion energy level as condition A (of Fig. 2 and Fig. 7 (a-b). This confirms that the inactivated AFM tip does not have a strong interaction with DNAloaded crystals. However, when normalized by interaction area, the interaction energy per area is not different from the non-reduced experiment, because the average penetration depth for tips that were preloaded with DNA was only 5.8 nm whereas the average penetration depth for tips that acquired DNA from inside the crystal is 22.9 ± 7.3 nm. This suggests that reduction with TCEP (with an average penetration depth of 9.90 nm) was insufficient to eliminate the tip-DNA interactions. For comparison, the average penetration depth was 13.22 nm and 5.96 nm for un-modified and activated tips, respectively, on unloaded crystals. The difference of penetration depth will directly lead to the difference of effective area of interaction, and therefore affect the total adhesion energy. Future single-molecule studies could further elucidate the interactions of individual dsDNA with protein crystal surfaces and pores.

To further confirm that the strong affinity seen with active tips and DNA-loaded crystals was due to DNA bound to the tip surface, we conjugated DNA directly to the tips rather than allowing activated tips to capture DNA from the crystal (case E in Figs. 2 and 7). The DNA-conjugated tips did not penetrate as far into the pores as unmodified tips. The solution-based conjugation of DNA to the tips (Fig. 7 (case E)) resulted in significantly higher adhesion energy per area than tips lacking DNA, and the nanopore pixels were clearly different from the wall pixels. The normalized adhesion energy per unit area was comparable to cases B and C, where DNA was first loaded into the crystals, and retrieved with activated tips. Further evidence for the strong interaction between the DNA and the protein crystals is provided by comparing cases B and E to case D, in which an activated tip was used in the absence of DNA. In this case we

found that the adhesion energy for the pore and wall areas and the normalized adhesion energy were similar to values found for the unmodified tip with no DNA.

Literature suggests that the mechanical force needed to rupture a disulfide bond may be 3.8 nN.³² Therefore the peak force used in these experiments was set to about 50% of this value (2 nN). For each extension-retraction trace, in addition to extracting the adhesion energy, we can calculate the maximum force (maximum difference between the extension and retraction curves). A box plot for these maximum force values corresponding to Fig. 7 is shown in Supporting Information Fig. S7. The value of maximum force was in a range of 760.4 pN (min) to 2029.8 pN (max), and the mean maximum force was 1509.5 pN, well below the force needed for mechanical disulfide rupture. Furthermore, this force is likely distributed among multiple DNA molecules bound to the tip and interacting with the crystal. Similarly, the maximum force observed across DNA-modified AFM tip with unloaded protein crystal's extension-retraction traces was 2029.8 pN. Therefore, we expect that DNA molecules that successfully conjugate to the tip will typically remain conjugated for many subsequent AFM tip oscillations. To confirm this, we have verified that the AFM tip that was pre-conjugated with DNA (pores in condition E of Figs. 2 and 7) had a mean adhesion energy of 1.68 \times 10-2 fJ for the first 10 nanopores imaged and a mean adhesion energy of 1.70×10^{-2} fJ for the last 10 nanopores imaged, 16 minutes later. In accord with this quantitative test, we further noted no overall trend in the adhesion energies collected with this tip over the course of the 16-minute image collection. The inverse experiment is to look for a chronological trend in the adhesion energies for the center of nanopores scanned with the tip that was activated but not explicitly loaded with DNA prior to the AFM scan. It is conceivable that the first nanopores might have a systematically lower adhesion energy due to the AFM tip not yet having conjugated a full complement of DNA molecules. However, in fact we observed no statistically significant difference between the first 20 nanopores (mean adhesion energy was 2.48×10^{-2} fJ), the subsequent 20 nanopores (mean adhesion energy was 2.47×10^{-2} fJ), and the last 20 nanopores (mean adhesion energy was 2.41×10^{-2} fJ) (Supporting Information Fig. S8). We therefore conclude that the AFM tip in this experiment (pores of condition B in Figs. 2 and 7) had ample time to conjugate to DNA during the setup time prior to the beginning of the image collection. As shown in Fig. 7 (a-b), there is a large difference in the adhesion energy on a per-pore basis, and these adhesion energies are quite consistent between neighboring pixels within a given pore, including pixels that are present on different horizontal scan lines, but there is no obvious correlation between nanopores that are probed consecutively. It is remarkable that individual pores demonstrate a consistent attachment strength when the tip returns to the nanopore on subsequent scan lines (~1000 milliseconds later). This implies that neither the composition of the tip nor the environment inside the nanopore is significantly varying on the 1000-millisecond timescale. This further supports the case that the DNA complement of the tip is not changing on a timescale that exceeds a typical expected time to move from one nanopore to the adjacent nanopore during the peak force scan.

The sinusoidal vertical oscillation profile used in the PeakForce QNM mode (as opposed to a linear ramp, used in typical force-volume mapping) ensures that the vertical tip velocity approaches a minimum of 0 as the tip reaches its fully extended position.

Therefore, at the tap frequencies (1kHz) used, the AFM tip will dwell within 1 nm of the maximum extension into the nanopores for approximately 52 microseconds and will be moving at a maximum velocity of less than $20 \cdot \pi$ nm/millisecond while the tip is within 10 nm of the maximum extension into the nanopores. At these speeds, we expect the short DNA molecule(s) that are conjugated to the AFM tip and submerged within the nanopores will have ample time to sample alternative molecular conformations and equilibrate with their local crystalline environment. This is consistent with the low intra-pore variation. To verify that the DNA had sufficient time to equilibrate (and thereby find conformations with maximal affinity for the local protein crystal matrix), we also performed peak force scans with a tap frequency of 2.0 kHz. Despite decreasing the time for DNA to equilibrate, no change was observed in the mean adhesion energy, nor in the mean number of retraction trace minima. (Supporting Information Fig. S5 and Table S3)

In theory, the maximum interaction of DNA with protein crystals could be recorded only when the AFM tips that bind with DNA were retracted from the center of the pores. The adhesion energy map Supporting Information Fig. S11 (b) emphasized this conclusion, there was a clear correspondence between the position of the strong interaction and the position of the nanopores. Therefore, to further understand this process, we expanded the number of randomly selected F-D curves per nanopore with an activated AFM tip on the crystal loaded with DNA to 5328, and all samples were from different individual nanopores. By finding and counting the zero point(s) of the first derivative on each retract force curve, we can further obtain the number of minima on each retract force curve. One of the interesting features observed in the F-D curves was multiple minima in the retraction (Fig. 6 (a-c) and Fig. S11 (d)). We hypothesize that these would be related to the formation of stronger specific DNA-crystal interactions during retraction. Each of the minima on the retract curve could represent a single interaction of a DNA molecule and a binding site on the protein crystal. 58.4% of the retract curves contained between 1 and 4 minima. The distributions of adhesion energies and number of retract curve minima are similar. Meanwhile, the adhesion energy distribution of F-D retract curves with different numbers of minima in Fig. S11 (e), shows no trend or obvious correlation between the number of minima and total adhesion energy. Among all the samples, over 99% of adhesion energy measurements were less than 6.0×10^{-2} fJ, 78.3% of adhesion energy measurements were concentrated in the 1.0×10^{-2} to 4.0×10^{-2} 10⁻² fJ range, and 50% of the adhesion energy values were between 1.60×10^{-2} and 3.29×10^{-2} fJ. F-D curves with total adhesion energy between 2.0×10^{-2} and 3.0×10^{-2} fJ account for 31.3%, which was the range where the adhesion energy was most concentrated among all the samples. The mean adhesion energy among all samples was 2.77 \times 10⁻² fJ. The maximum adhesion energy recorded was 8.77 \times 10⁻² fJ. The comparison to condition A (non-activated tip) and case D (activated tip), which were conducted in the absence of DNA, shows that the majority of this interaction energy should be attributed to the DNA-crystal interaction. Additional interactions that could also contribute include potential friction forces with the inner walls of protein crystals.

Conclusions

For the first time, the porous surface structure of this unusual type of protein crystal was observed, and imaged in the liquid phase via high-resolution AFM, revealing details of the porous crystal surface. In this study, DNA was successfully loaded into protein crystals. Loading and strong adhesion were confirmed by confocal microscope imaging. All the AFM data was likewise consistent with the confocal microscope imaging in confirming a strong interaction of DNA with CJ protein crystals. As intended, DNA-modified AFM tips had a dramatically stronger interaction with the crystal nanopores, presumably via the extra work associated with extracting DNA from the crystal during retraction. Our optimized AFM characterization quantitatively measures and analyzes the mechanical behaviors, and the nano-scale variations in the adhesion energy between DNA and protein crystals. We therefore propose that this method could be used more generally to study the interactions between guest molecules and porous crystals, such as interaction of polyethylene glycol-arginylglycylaspartic acid complex with porous protein crystals. In the future, we propose to use machine learning to process and classify the hundreds of thousands of F-D curves we have collected. We expect that this analysis will provide further insights into how objects that present multiple DNA strands will interact with protein crystals. In turn, this knowledge will advance our understanding of CJ protein crystals as capable and reliable DNA containers, and provide a basis for engineering functional biomaterials that are responsive to small pulling forces.

Author Contributions

Dafu Wang: data curation, investigation, methodology, writing; Julius D. Stuart: investigation, methodology, writing; Alec A. Jones: investigation; Christopher D. Snow: conceptualization, formal analysis, funding acquisition, methodology, project administration, supervision, visualization, writing; and Matt J. Kipper: conceptualization, formal analysis, funding acquisition, methodology, project administration, supervision, writing.

Conflicts of Interest

There are no conflicts to declare.

Acknowledgements

The authors greatly appreciate the support of National Science Foundation Grant CBET/BEINM-1704901. The authors also thank Dr. Ann E. Kowalski and Ms. Abigail R. Ward for their generous help and patient guidance on crystal preparation.

References

- 1. L. F. Hartje, B. Munsky, T. W. Ni, C. J. Ackerson and C. D. Snow, *J. Phys. Chem. B*, 2017, **121**, 7652-7659.
- T. R. Huber, L. F. Hartje, E. C. McPherson, A. E. Kowalski and C. D. Snow, *Small*, 2017, 13, 1602703.
- 3. T. R. Huber, E. C. McPherson, C. E. Keating and C. D. Snow, *Bioconjugate Chem.*, 2017, 29, 17-22.

- A. E. Kowalski, T. R. Huber, T. W. Ni, L. F. Hartje, K. L. Appel, J. W. Yost, C. J. Ackerson and C. D. Snow, *Nanoscale*, 2016, 8, 12693-12696.
- B. P. Brown, L. Picco, M. J. Miles and C. F. Faul, Small, 2013, 9, 3201-3211.
- 6. E. C. Beckwitt, M. Kong and B. Van Houten, 2017.
- Y. F. Dufrene, T. Ando, R. Garcia, D. Alsteens, D. Martinez-Martin, A. Engel, C. Gerber and D. J. Muller, *Nat. Nanotechnol.*, 2017, 12, 295-307.
- D. Yamamoto, N. Nagura, S. Omote, M. Taniguchi and T. Ando, *Biophys. J.*, 2009, **97**, 2358-2367.
- K. YuG, A. Malkin, T. Land, J. DeYoreo, A. Barba, J. Konnert and A. McPherson, *Biophys. J.*, 1997, 72, 2357-2364.
- M. Hedayati, D. F. Marruecos, D. Krapf, J. L. Kaar and M. J. Kipper, *Acta Biomater.*, 2020, **102**, 169-180.
- M. Hedayati, M. M. Reynolds, D. Krapf and M. J. Kipper, ACS Appl. Mater. Interfaces, 2018, 10, 31892-31902.
- M. Pfreundschuh, D. Martinez-Martin, E. Mulvihill, S. Wegmann and D. J. Muller, *Nat. Protoc.*, 2014, 9, 1113.
- 13. A. E. Lopez, S. Moreno-Flores, D. Pum, U. B. Sleytr and J. L. Toca-Herrera, *Small*, 2010, **6**, 396-403.
- S. D. Durbin, W. E. Carlson and M. Saros, J. Phys. D: Appl. Phys., 1993, 26, B128.
- 15. T. Keel, University of Nottingham, 2004.
- A. Malkin, Y. G. Kuznetsov and A. McPherson, Surf. Sci., 1997, 393, 95-107.
- D. Caballero, J. Samitier, J. Bausells and A. Errachid, *Small*, 2009, 5, 1531-1534.
- C. Liang, Z. Ye, B. Xue, L. Zeng, W. Wu, C. Zhong, Y. Cao, B. Hu and P. B. Messersmith, ACS Appl. Mater. Interfaces, 2018, 10, 25017-25025.
- H. Lee, N. F. Scherer and P. B. Messersmith, *Proc. Natl. Acad. Sci.*, 2006, **103**, 12999-13003.
- Y. Zhang, Y. Miyahara, N. Derriche, W. Yang, K. Yazda, X. Capaldi, Z. Liu, P. Grutter and W. Reisner, Small Methods, 2019, 1900147.
- C. S. Goldsbury, S. Scheuring and L. J. C. p. i. p. s. Kreplak, 2009, 58, 17.17. 11-17.17. 19.
- 22. A. Pyne, R. Thompson, C. Leung, D. Roy and B. W. Hoogenboom, *Small*, 2014, **10**, 3257-3261.
- H. Li, M. A. Perozzo, J. H. Konnert, A. Nadarajah and M. L. Pusey, Acta Crystallogr. D Biol. Crystallogr., 1999, 55, 1023-1035.
- 24. H. Yamashita, K. Voitchovsky, T. Uchihashi, S. A. Contera, J. F. Ryan and T. Ando, *J. Struct. Biol.*, 2009, **167**, 153-158.
- M. Bergkvist and N. C. Cady, in *Bioconjugation Protocols*, Springer, 2011, pp. 381-400.
- D. Anselmetti, J. Fritz, B. Smith and X. Fernandez -Busquets, Single Mol., 2000, 1, 53-58.
- L. Lin, H. Wang, Y. Liu, H. Yan and S. Lindsay, *Biophys. J.*, 2006, **90**, 4236-4238.
- M. Hedayati and M. J. Kipper, Carbohydr. Polym., 2018, 190, 346-355.
- J. P. Killgore, R. H. Geiss and D. C. Hurley, Small, 2011, 7, 1018-1022.
- 30. B. V. Crist and D. B. Crisst, *Handbook of monochromatic XPS spectra*, Wiley New York, 2000.
- 31. B. V. Crist, XPS Reports, 2007, 1.
- 32. M. F. lozzi, T. Helgaker and E. Uggerud, *J. Phys. Chem. A*, 2011, **115**, 2308-2315.